5-1-2022

Large-Eddy Simulations of a Convection Cloud Chamber: Sensitivity to Bin Microphysics and Advection

Fan Yang
Brookhaven National Laboratory

Mikhail Ovchinnikov
Pacific Northwest National Laboratory

Subin Thomas
Michigan Technological University, subint@mtu.edu

Alexander Khain
Hebrew University of Jerusalem

Robert McGraw
Brookhaven National Laboratory

See next page for additional authors

JAMES | Journal of Advances in Modeling Earth Systems

RESEARCH ARTICLE
10.1029/2021MS002895

Large-Eddy Simulations of a Convection Cloud Chamber: Sensitivity to Bin Microphysics and Advection

Fan Yang[1], Mikhail Ovchinnikov[2], Subin Thomas[3], Alexander Khain[4], Robert McGraw[1], Raymond A. Shaw[3], and Andrew M. Vogelmann[1]

[1]Brookhaven National Laboratory, Upton, NY, USA, [2]Pacific Northwest National Laboratory, Richland, WA, USA, [3]Michigan Technological University, Houghton, MI, USA, [4]Department of Earth Sciences, Hebrew University of Jerusalem, Jerusalem, Israel

Abstract Bin microphysics schemes are useful tools for cloud simulations and are often considered to provide a benchmark for model intercomparison. However, they may experience issues with numerical diffusion, which are not well quantified, and the transport of hydrometeors depends on the choice of advection scheme, which can also change cloud simulation results. Here, an atmospheric large-eddy simulation model is adapted to simulate a statistically steady-state cloud in a convection cloud chamber under well-constrained conditions. Two bin microphysics schemes, a spectral bin method and the method of moments, as well as several advection methods for the transport of the microphysical variables are employed for model intercomparison. Results show that different combinations of microphysics and advection schemes can lead to considerable differences in simulated cloud properties, such as cloud droplet number concentration. We find that simulations using the advection scheme that suffers more from numerical diffusion tends to have a smaller droplet number concentration and liquid water content, while simulation with the microphysics scheme that suffers more from numerical diffusion tends to have a broader size distribution and thus larger mean droplet sizes. Sensitivities of simulations to bin resolution, spatial resolution, and temporal resolution are also tested. We find that refining the microphysical bin resolution leads to a broader cloud droplet size distribution due to the advection of hydrometeors. Our results provide insight for using different advection and microphysics schemes in cloud chamber simulations, which might also help understand the uncertainties of the schemes used in atmospheric cloud simulations.

Plain Language Summary We investigate the dependence of high-resolution cloud simulations on the algorithms used to represent the cloud microphysics and advective transport. The model setup is constrained and guided by observed steady-state clouds in a convection cloud chamber. Two bin microphysics algorithms along with several advection methods are used to simulate the clouds with the same initial and boundary conditions. All simulations reach a steady state, and considerable intermodel variations in simulated cloud properties are found when using different advection and microphysics schemes. The case-by-case variations show some correlations with the estimated degree of numerical diffusion suffered by different schemes. Results from model intercomparisons help better understand uncertainties in simulations of clouds in the chamber and in the real atmosphere.

Key Points:

- Large-eddy simulations of a convection cloud chamber are conducted using several microphysics and advection schemes
- Changes in advection schemes can produce similar variability in simulated cloud properties as do changes in the microphysics schemes
- Refining microphysical bin widths leads to a broader droplet size distribution due to the advection of hydrometeors

Supporting Information:

Supporting Information may be found in the online version of this article.

Correspondence to:

F. Yang,
fanyang@bnl.gov

Citation:

Yang, F., Ovchinnikov, M., Thomas, S., Khain, A., McGraw, R., Shaw, R. A., & Vogelmann, A. M. (2022). Large-eddy simulations of a convection cloud chamber: Sensitivity to bin microphysics and advection. *Journal of Advances in Modeling Earth Systems*, *14*, e2021MS002895. https://doi.org/10.1029/2021MS002895

Received 3 NOV 2021
Accepted 8 MAY 2022

Author Contributions:

Conceptualization: Fan Yang, Mikhail Ovchinnikov, Subin Thomas, Raymond A. Shaw
Investigation: Fan Yang
Methodology: Fan Yang, Mikhail Ovchinnikov, Alexander Khain, Robert McGraw
Software: Fan Yang
Validation: Fan Yang

1. Introduction

Clouds play a crucial role in the Earth's energy balance by reflecting solar radiation and absorbing terrestrial radiation. They are also important to the hydrological cycle through precipitation and water redistribution in the atmosphere. A better representation of clouds in atmospheric models can improve weather forecasts and climate projections. One challenge of cloud simulation is to accurately represent cloud properties and processes under various conditions. The challenge arises from limited understanding of complicated cloud microphysical processes at the fundamental level, as well as from imperfect translation of this understanding to the numerical algorithms used to resolve or parameterize microphysical processes (e.g., Khain et al., 2015; Morrison et al., 2020).

In general, there are three approaches to simulate microphysical properties of hydrometeors and related processes in atmospheric models: bulk representation of particle properties, bin microphysical schemes, and Lagrangian particle methods. Bulk microphysics schemes use one or more attributes (e.g., moments of the hydrometeor size

Writing – original draft: Fan Yang
Writing – review & editing: Mikhail Ovchinnikov, Alexander Khain, Robert McGraw, Raymond A. Shaw, Andrew M. Vogelmann

distribution) to represent the volume-average properties of each type of hydrometeor (e.g., cloud droplets, rain drops, and ice particles). Bin microphysical schemes partition the particle size distribution into typically a few tens of discretized sections (or bins) to cover a wide range of hydrometeor sizes, from cloud droplets of a few micrometers to rain drops of several millimeters. Hydrometeors in each bin are quantified by one or more attributes (e.g., number and/or mass mixing ratio per bin). Lagrangian particle-based methods have been extensively developed in the past decade (e.g., Hoffmann et al., 2015; Grabowski et al., 2019, Shima et al., 2009, and references therein). This method tracks hundreds of thousands of "superdroplets", with each superdroplet representing an ensemble of hydrometeors with the same properties (e.g., size, mass, phase).

Various bulk and bin microphysics schemes have been developed and used for cloud simulations. For example, Khain et al. (2015) summarize the main characteristics of over 40 previous studies using bulk microphysics schemes (Table 2 in their paper) and over 20 previous studies using bin microphysics schemes (Table 3 in their paper). One way to understand the spread and uncertainties of different microphysics schemes is through model intercomparison studies in which different models simulate a cloud using the same initial and boundary conditions. Significant intermodel variations have been found in the simulations of different types of clouds, for example, shallow cumulus cloud (e.g., VanZanten et al., 2011), stratocumulus cloud (e.g., Stevens et al., 2005), mixed-phase clouds (e.g., Ovchinnikov et al., 2014), and deep convective clouds (e.g., Xue et al., 2017).

Generally speaking, by allowing the droplet size distribution to evolve freely under various processes, the bin microphysical schemes have the ability to represent cloud microphysical properties and processes more accurately compared with bulk microphysics schemes, which usually assume a specific shape of droplet size distribution. Consequently, high-resolution bin schemes are often used as the standard for evaluation of the more approximate bulk schemes. However, often intermodel variations also exist when using different bin microphysics schemes, and it is important to determine how much of these differences are due to different bin microphysics schemes rather than other factors, such as different dynamic frameworks, advection schemes, and subgrid-scale parameterizations. In this regard, kinematic models that remove certain dynamics and dynamical feedbacks to simplify such intercomparisons have been developed (e.g., Hill et al., 2015; Shipway & Hill, 2012). In a dynamic system, simulated cloud properties can be affected by the choice of cloud microphysics scheme as well as the interactions and feedbacks among microphysics, thermodynamics, and dynamics. For example, Morrison et al. (2018) found that the vertical advection of hydrometeors can be affected by numerical diffusion resulting in an artificially enhanced broadening of the cloud droplet size distribution. Recently, Pardo et al. (2020) explored the broadening of droplet size distribution in an idealized cumulus cloud and they found that physical broadening mechanisms (e.g., activation, collision, entrainment, and mixing) are more important than the artificial broadening mechanism.

The complex dynamic system presents a challenge to isolate and quantify the role of the microphysics scheme, especially when various microphysical and dynamical numerical schemes are used in different models. While free-running simulations with different microphysics schemes produce different results, the interpretation is complicated and effects may be hidden or amplified by numerous feedbacks during cloud evolution. Using the same dynamics with different microphysics schemes or the same microphysics in different dynamical frameworks can expose some glaring issues, but reasons for more subtle differences are difficult to diagnose (Ovchinnikov & Ghan, 2005). Constraining dynamics further, by using either a kinematic framework or "piggybacking" (offline microphysics) (Grabowski, 2019), prevents microphysics-dynamics feedbacks, which expose differences in microphysics more clearly. One of the potential downsides or limitations of this decoupling is that one may not end up in a relevant area of the parameter space because of inconsistencies between dynamics, which provide the forcing, and the microphysics itself.

Clouds have been generated in chamber facilities to investigate their fundamental physical and chemical properties and processes under well-constrained laboratory conditions. Steady-state clouds generated under well-characterized boundary conditions hardly exist in the atmospheric context, thereby making atmospheric cloud simulation results tricky to interpret. A convection-cloud chamber, in which turbulence is constantly forced and well characterized, provides a unique opportunity to explore aerosol-cloud-turbulence interactions. For example, the convection-cloud chamber at Michigan Technological University (called the Pi Chamber), which generates turbulence through Rayleigh-Bènard convection by maintaining a warm lower surface and cold upper surface, can form and maintain a turbulent cloud in a steady state for many hours (e.g., Chandrakar et al., 2016; Chang et al., 2016). The Leipzig Aerosol Cloud Interaction Simulator (LACIS-T) is another cloud chamber in which turbulent cloud is generated by mixing two airflows in a wind tunnel (Niedermeier et al., 2020).

The cloud microphysics schemes used for atmospheric cloud simulations should also be applicable to the simulation of clouds in the chamber because the fundamental physics that controls the microphysical processes, such as droplet activation and condensational growth, is the same. Simulations of clouds at laboratory scale were rare, especially in a turbulent environment, until recently when turbulent chambers became operational. For example, a computational fluid dynamics software OpenFOAM with Lagrangian particles has been used to simulate clouds in LACIS-T (Niedermeier et al., 2020), and the System for Atmospheric Modeling (SAM, Khairoutdinov & Randall, 2003) with a spectral bin microphysics scheme based on Khain et al. (2004) (a scheme developed at Hebrew University of Jerusalem, Israel, hereafter referred to as the HUJI scheme) has been modified to simulate clouds in the Pi chamber (Thomas et al., 2019). One conclusion from the "Workshop to Explore Science Opportunities and Concepts for a Large-Scale Aerosol–Cloud–Turbulence Research Facility", held in November 2019 at Boulder, is that a laboratory facility can provide a well-constrained and observationally guided state for model simulation and intercomparison (Shaw et al., 2020). Laboratory-constrained and evaluated cloud models can help to reduce the uncertainties in aerosol-cloud-turbulence interactions in large-scale models.

Here, we perform a comparison of large-eddy simulations of cloud in the Pi chamber using two bin microphysics schemes and multiple advection schemes for hydrometeor transport. A unique aspect of this intercomparison is that the model setup allows us to produce a steady-state cloud in a well-constrained dynamic system, which removes time evolution from consideration and yet allows all feedbacks between the dynamics and microphysics to operate. We note that bin microphysics spectral broadening related to vertical advection, which may be an important concern for modeling "real clouds" (Morrison et al., 2018), does not manifest itself in our setup because the condensation in a convection chamber is driven by supersaturation generated by isobaric mixing and not by adiabatic expansion tied to the vertical advection (Grabowski, 2020). The idealized simulation framework enables comparison of the relative contributions to the simulations of the microphysics and advection schemes and can also help with the design of laboratory experiments to evaluate and constrain numerical methods in the future. We will show that both the microphysics and advection schemes can alter the statistical properties (e.g., mean droplet number concentration) of simulated clouds in the Pi Chamber. Similar cloud properties can result from using different combinations of microphysics and advection schemes. We also find that refining the microphysical bin widths leads to a broader cloud droplet size distribution due to the transport of hydrometeors. This broadening effect might also exist in atmospheric cloud simulations. The model description and setup are detailed in Section 2. Results are discussed in Section 3, followed by the conclusions.

2. Model Description and Setup

The dynamical model we use is the SAM (Khairoutdinov & Randall, 2003) modified for large-eddy simulation of cloud in the Pi Chamber. The model setup including initial and boundary conditions are described in detail by Thomas et al. (2019) and is briefly summarized here. The domain size is 2 m × 2 m × 1 m (height) with a resolution of 3.125 × 3.125 × 3.125 cm (a total of 64 × 64 × 32 grid boxes). The floor temperature is set as 299 K, the ceiling temperature is 280 K, and the wall temperature is 285 K. The floor and ceiling surfaces are water saturated, and the sensible and latent heat fluxes are calculated based on the Monin-Obukhov similarity theory. Side-wall sensible and latent heat fluxes are calculated using the same parameterization. The wall surface wetness is set to be 0.78 (0.78 times its saturated value), such that the domain-averaged supersaturation in steady state without cloud droplets is about 2.5%, which is close to in situ measurements in the Pi Chamber (Chandrakar et al., 2016). Note that our calculation of side-wall fluxes is the only way to adjust the domain-averaged supersaturation to match the in situ observations. More advanced models, such as wall-modeled LES and direct numerical simulation, are needed to calculate the surface fluxes at the process level. The total simulation is 1 hr with a time step of 0.02 s. Domain-averaged variables (e.g., temperature, water vapor mixing ratio) are output every 1 s for time series plots. Instantaneous 3D microphysics fields are output after the first half an hour at 5 min intervals. Therefore, a total of seven instantaneous 3D fields are used to calculate the spatial- and domain-averaged droplet size distribution.

2.1. Cloud Microphysics Schemes

Two bin microphysics schemes are used in this study: the HUJI scheme based on Khain and Sednev (1996), and the scheme based on microphysical method of moments developed by Chen and Lamb (1994), hereafter referred to as the CL scheme. In the HUJI scheme, aerosol and different types of hydrometeors are each represented by

33 doubling-mass bins. In each bin, the mass mixing ratio of cloud droplet is the prognostic variable, while the number mixing ratio is diagnosed from the mean size which is fixed. The HUJI scheme is also called a spectral bin microphysics scheme (Khain et al., 2015). The HUJI scheme has been modified and applied in different dynamical models to simulate atmospheric clouds, such as the Hebrew University Cloud Model (e.g., Khain et al., 2004), the NCAR Mesoscale Model (e.g., Lynn et al., 2005), the SAM (e.g., Fan et al., 2009), and the Weather Research and Forecasting Model (e.g., Khain et al., 2010).

The CL bin microphysics scheme is based on the microphysical method of moments in which both mass mixing ratio and number mixing ratio in each bin are prognostic variables. It has been recently used in a cloud parcel model to simulate optically thin clouds (Kuan-Ting et al., 2018). In this study, we also use 33 bins to represent cloud droplets as in the HUJI scheme. The bin boundaries are organized in a doubling-mass coordinate starting from 1 μm. In each bin, the droplet size distribution is represented by a linear mass-dependent function, and the mean size (mass) of cloud droplets can vary between its left and right bin boundaries. Similarly, newly activated cloud droplets are added to the smallest cloud droplet bin. For condensational growth and evaporation, the linear distribution in each mass bin will shift to the larger size (growth) or smaller size (evaporation), and then remap back to the original grid coordinate. Details of the bin shift and remapping methods can be found in Chen and Lamb (1994).

Monodisperse aerosol particles are injected uniformly in every grid box at every time step as in Thomas et al. (2019). For the basic setup, the aerosol injection rate is 0.25 $cm^3 s^{-1}$. Aerosol particles are composed of sodium chloride with a dry diameter of 125 nm. Volume aerosol injection (i.e., injection at every grid box) is chosen for this study to minimize the influence of aerosol transport on cloud activation when using different scalar advection schemes. A similar strategy of volume aerosol injection has been used in Grabowski (2020). An aerosol particle is activated into a cloud droplet if the supersaturation in the grid box is higher than its critical supersaturation (~0.054%). After newly activated cloud droplets are added to the smallest cloud droplet bin, cloud droplets then grow by condensation under supersaturated conditions and evaporate under subsaturated conditions. There are two ways to remove droplets from the simulation domain: evaporation, when the droplet radius is smaller than 1 μm, and sedimentation, at the bottom surface. Sedimentation is controlled by the droplet terminal velocity and, in this study, terminal velocity of the mean droplet size in each bin is calculated based on Beard (1976). For simplification, droplets are not removed by the side-wall surfaces; this is accomplished by forcing the hydrometeor fluxes at the side-wall surfaces to be zero. A dynamic steady state is reached when the source of cloud droplets due to activation is balanced by the sink due to sedimentation. Collision-coalescence is ignored because the estimated collision time scale (~1 hr or larger) is much longer than the droplet residence time (a few minutes) in the Pi Chamber due to the limited vertical extent (1 m) (Chandrakar et al., 2016). Aerosol reactivation and scavenging processes are also ignored for simplification. It should be mentioned that, although there are some similarities in microphysics treatment between this study and Grabowski (2020), it is difficult to make quantitative comparisons between the simulations, because the side-wall conditions and surface flux calculation are handled quite differently and can have a significant impact on cloud properties. For a better comparison, the same or similar initial and boundary conditions are needed for the model setup. In a recent international cloud modeling workshop, different models were brought together to simulate the Pi chamber with specific guidance of the model setup (Xue et al., 2022). These comparisons of the Pi chamber simulations among different models are expected to be published in the future.

2.2. Advection Schemes for Hydrometeors

Besides the cloud microphysics scheme itself, another factor that can influence the accuracy of a cloud simulation is the advection scheme which controls the transport of hydrometeors in space (Olesik et al., 2021). Various numerical advection algorithms have been developed and used in atmospheric models (Rood, 1987). Although suffering from numerical diffusion, first-order linear advection schemes are efficient and can preserve the correlations among sets of advected scalars, which are important in transporting aerosol mixtures and chemical tracers (McGraw, 2007). Higher-order advection schemes can reduce the numerical diffusion but might cause other issues, such as unrealistic negative values and oscillations in the advected variable values, especially close to a sharp boundary. Various nonlinear terms and corrections have been developed and applied to high-order advection schemes to enforce nonoscillation and monotonic properties; however, they increase the computational cost and cannot maintain the interrelationship among advected variables (Ovchinnikov & Easter, 2009).

The advection scheme used in our previous Pi Chamber simulation (Thomas et al., 2019) is the multidimensional positive definite advection transport algorithm (MPDATA) with the nonoscillatory option (Smolarkiewicz & Grabowski, 1990). The default MPDATA scheme is suitable for the advection of hydrometeors in the HUJI scheme but is not suitable for the CL scheme. To explain this point, we use M_i and N_i to represent the mass and number mixing ratio in bin i. In the HUJI scheme, M_i is a prognostic variable, while N_i is a diagnostic variable calculated from the ratio of M_i and bin i's drop size, which is a constant. For the CL scheme, both M_i and N_i are prognostic variables, and the mean drop size varies within bin i. The problem is that, after advection, the mean size of the droplet in bin i, given by the ratio of M_i and N_i, might be smaller than at the left boundary or larger than at the right boundary of bin i. This is because a nonlinear, high-order advection scheme, like MPDATA, cannot preserve the interrelationship of advected variables, as discussed in Ovchinnikov and Easter (2009). Therefore, number or mass adjustments might be needed when using a moment-based bin microphysics scheme together with a high-order, nonlinear advection scheme. For example, Yamaguchi et al. (2019) simulated shallow convection clouds using a monotonic, fifth-order advection scheme (Yamaguchi et al., 2011) and the Tel Aviv University (TAU) bin microphysics scheme, which is similar to the CL scheme in that both M_i and N_i are prognostic variables as detailed in Tzivion et al. (1987). In the simulations, the cloud droplet number concentration is adjusted before computing the microphysics when the number concentration is negative, caused by the nonlinear nature of their high-order scalar advection scheme. Below, we provide three different advection methods for the CL scheme to maintain the interrelationship between M_i and N_i after advection.

2.2.1. MPDATA With Mass Adjustment

In this method, both M_i and N_i are advected using MPDATA. If M_i/N_i does not fall into bin i after advection, we keep N_i the same but do the following adjustments: (a) if M_i/N_i is smaller than the value at the bin i's left boundary, we modify M_i to M_i^* such that M_i^*/N_i is equal to the value at the bin i's left boundary plus 0.01 of bin i's width; (b) if M_i/N_i is larger than the value at the bin i's right boundary, we modify M_i to M_i^* such that M_i^*/N_i is equal to the value at the bin i's right boundary minus 0.01 of bin i's width. This mass-adjustment strategy is inspired by the TAU bin microphysics scheme developed by Tzivion et al. (1987) (e.g., Equations 15a, 15b in their paper). However, we note that the correction in Tzivion et al. (1987) is made for cases when the mean size is not well defined due to very tiny mass and number concentration in a bin, not for advection corrections. It should be mentioned that the total condensed water in the simulation domain is not conserved after advection if mass is adjusted. To explore the impact of mass adjustment, we develop a mass-conserved adjustment method that is detailed in the following subsection.

2.2.2. MPDATA With Number Adjustment

In this method, only M_i is advected using MPDATA while N_i is adjusted as discussed below. After advection, some grid boxes lose number and mass in bin i, while the other grid boxes gain number and mass in bin i. We use δM_i (+) and δN_i(+) (δM_i (−) and δN_i(−)) to represent the gain (loss) of mass and number mixing ratios in bin i. If one grid box loses mass concentration in bin i (δM_i (−)), the loss of the number concentration in that bin can be calculated as

$$\delta N_i(-) = \frac{\delta M_i(-)}{m_{i,old}} \tag{1}$$

where $m_{i,\mathrm{old}}$ is the mean droplet size in bin i in that grid box in the previous time step. For grid boxes gaining number and mass, we define m^* as the characteristic droplet mass in bin i during advection,

$$m^* = \frac{\sum \delta M_i(-)}{\sum \delta N_i(-)}, \tag{2}$$

and the increase of number concentration in a mass-gaining grid box can be calculated as

$$\delta N_i(+) = \frac{\delta M_i(+)}{m^*} \tag{3}$$

the assumptions we made here are given as follows: (a) for grid boxes losing number and mass, they lose droplets with the droplet mass of the previous time step; and (b) for grid boxes gaining mass, they gain droplets with

Table 1
A Summary of Cases With Various Combinations of Microphysics and Advection Schemes

Case Name	Microphysics	Advection
H-M	HUJI	MPDATA
H-Sh	HUJI	Semi-Lagrangian (hybrid)
H-Sf	HUJI	Semi-Lagrangian (first-order)
C-Mm	CL	MPDATA (mass adjustment)
C-Mn	CL	MPDATA (number adjustment)
C-Sh	CL	Semi-Lagrangian (hybrid)

characteristic mass calculated based on Equation 2. One advantage of this adjustment is that the total droplet number in bin i within the whole domain is conserved after advection, because $\sum\delta N_i(+) = |\sum\delta N_i(-)|$.

2.2.3. Semi-Lagrangian Advection Scheme

Recently, an efficient semi-Lagrangian advection (SLA) scheme has been developed to transport cloud microphysical variables for cloud simulation in a 2-D kinematic field (Gavze et al., 2020) and a 3-D dynamic field (Lynn et al., 2021). Efficiency is one of the main advantages of the SLA scheme, especially in regard to computationally expensive cloud simulations using bin microphysics schemes. Results show that SLA can preserve the interrelationship between advected scalars, while SLA with a hybrid option also has a better agreement with other high-order advection schemes. In this study, we use the hybrid SLA scheme to transport M_i and N_i in the CL scheme. The hybrid SLA scheme is a combination of the first-order, semi-Lagrangian bilinear scheme and the second-order, semi-Lagrangian biquadratic scheme. We choose a weighting factor of 0.5, which has shown good agreement with other high-order, nonlinear advection schemes (Gavze et al., 2020). We also apply the first-order SLA scheme and the hybrid SLA scheme to transport M_i in the HUJI scheme. We note that Gavze et al. (2020) and Lynn et al. (2021) recommend against using the first-order SLA because of its large numerical diffusion. However, because the purpose of this study is to explore a range of variations in chamber simulations due to different schemes, we still employ the first-order SLA scheme with the HUJI for comparison.

2.3. Overview of Cases

All cases analyzed in this study are listed in Table 1. The first capital letter in the case name corresponds to the microphysics scheme: "H" is for the HUJI scheme, and "C" is the CL scheme. The second capital letter in the case name represents which advection scheme is used: "M" is for the MPDATA scheme and "S" is the semi-Lagrangian scheme. Specifically, "Sf" and "Sh" represents SLA with the first-order and hybrid options. Special treatment for CL cases are "Mm" and "Mn", in which either mass or number mixing ratio is adjusted as discussed in Sections 2.2.1 and 2.2.2.

Some schemes are more diffusive than others. For example, in the droplet size space, the HUJI scheme is more diffusive than the CL scheme, and in the position space, the first-order SLA scheme is more diffusive than the hybrid SLA scheme and the MPDATA scheme. However, it is difficult to predict the outcome of different combinations of microphysics and advection schemes due to complex interactions and nonlinear feedbacks among dynamics, thermodynamics, and microphysics. An objective of this study is to quantitatively show the case-by-case variations when using different combinations of schemes. One advantage of the SLA scheme, which is not the main focus of this study but is worth a mention, is its low computation cost compared with other advection schemes, as detailed in Gavze et al. (2020) and Lynn et al. (2021). Indeed, we find that the total simulation time when using the SLA scheme is about 60% of that using the MPDATA scheme. A surprising finding is that the total simulation time when using the CL scheme is about 35% of that when using the HUJI scheme. This finding contradicts our expectation, because the prognostic microphysical variables in CL (mass mixing ratio and number mixing ratio) are twice that in HUJI (mass mixing ratio only).

3. Results and Discussion

All simulations are conducted with the same initial and boundary conditions detailed in Section 2. For baseline intercomparisons, the aerosol injection rate is 0.25 $cm^{-3}\ s^{-1}$. We first evaluate the time evolution of the domain-averaged thermodynamic and microphysical variables, and then compare spatially and temporally averaged droplet size distributions in steady state for the various cases (Results in 3.1). Two larger aerosol injection rates (2.5 $cm^{-3}\ s^{-1}$ and 25 $cm^{-3}\ s^{-1}$) are used to investigate variations in relatively polluted conditions (Results in 3.2). As this is the first time the CL scheme has been implemented in SAM, we conducted additional simulations to explore the sensitivity to parameters used in the CL scheme (Results in 3.3). Finally, H-M and C-Mm are chosen to run at different spatial and temporal resolutions to check whether results depend on grid spacing and time step (Results in 3.4).

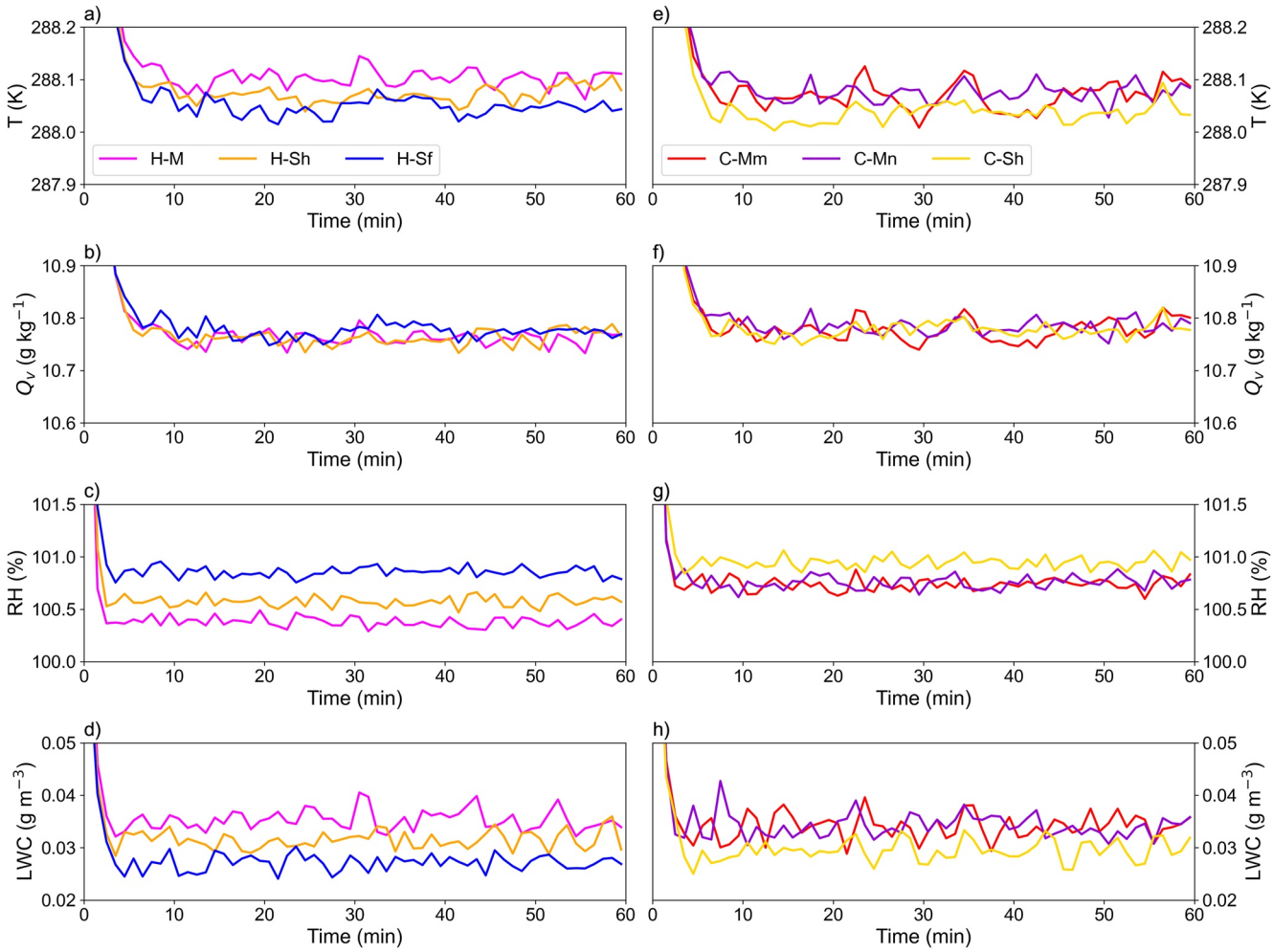

Figure 1. Time series of domain-averaged (a),(e) temperature (b),(f) water vapor mixing ratio (c),(g) relative humidity, and (d),(h) liquid water content in a simulated convection cloud chamber. Results in the left column use the HUJI microphysics scheme, and results in the right column use the CL microphysics scheme. The colors indicate different combinations of microphysics and advection schemes, as detailed in Table 1 and the main text. The aerosol injection rate is 0.25 cm^{-3} s^{-1}.

3.1. Comparisons Among Various Schemes at a Constant Aerosol Injection Rate

Figure 1 shows the time series of domain-averaged temperature (T), water vapor mixing ratio (Q_v), relative humidity (RH), and liquid water content (LWC) inside the chamber for an aerosol injection rate of 0.25 cm^{-3} s^{-1}. Results show that all variables reach a steady state after about 5 min. The H-M case uses the same microphysics and advection schemes as in Thomas et al. (2019). The energy dissipation rate is about 0.0014 m^2 s^{-3}, which is similar to that in stratocumulus clouds, and the turbulent kinetic energy is about 0.0011 m^2 s^{-2}. Details about the turbulence and flow properties for the Pi chamber simulation with a similar model setup can be found in Thomas et al. (2019). In this study, we mainly focus on the thermodynamic and microphysical properties as the advection and microphysics schemes are changed, because turbulence is not sensitive to those changes. The spatial resolution has a considerable impact on the turbulence, which will be discussed in Section 3.4.

Results in Figure 1 are plotted in order of the estimated degree of numerical diffusion (from low to high): H-M $\leq$ H-Sh $\leq$ H-Sf; C-Mm $\sim$C-Mn $\leq$ C-Sh. It is interesting to see that, when using the same microphysics scheme, simulation using an advection scheme that suffers more from numerical diffusion tends to have a lower T, higher RH, and smaller LWC. Q_v is not sensitive to the change in advection scheme. It should be mentioned that liquid water static energy and total water mixing ratio are the two prognostic variables in SAM. For all the cases, we use MPDATA to advect these two variables, and only hydrometeors are advected differently for comparison (e.g., MPDATA vs. SLA). The same strategy has been used in Lynn et al. (2021) to investigate the transport of

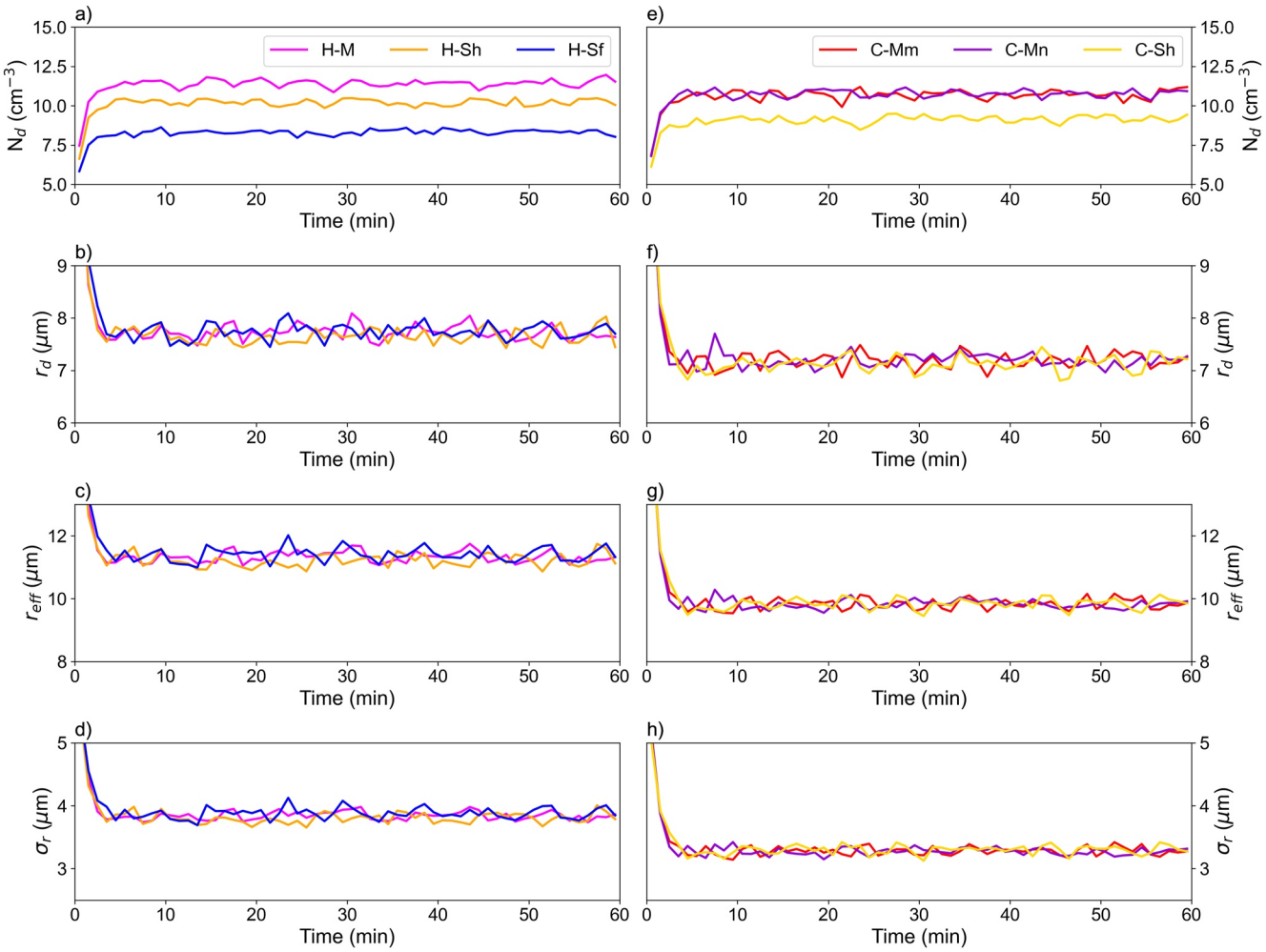

Figure 2. Time series of domain-averaged (a),(e) droplet number concentration (b),(f) mean droplet radius (c),(g) effective radius, and (d),(h) standard deviation of droplet size distribution in a simulated convection cloud chamber. Results in the left and right columns use the HUJI and CL microphysics schemes, respectively. The colors indicate different combinations of microphysics and advection schemes, as detailed in Table 1 and the main text. The aerosol injection rate is 0.25 cm^{-3} s^{-1}.

microphysical quantities using different advection schemes. Therefore, the differences we see here are mainly due to different ways the advection of hydrometeors is treated (when using the same microphysics scheme). For cross comparison, domain-averaged T is slightly lower and Q_v is slightly higher when using the CL scheme compared with the HUJI scheme (see Table S1 in Supporting Information S1); this leads to systematic differences in *RH* (the CL cases is higher than the HUJI cases) as shown in Figures 1c and 1g, except for H-Sf which is similar to the CL cases. The mean and variations in *LWC* are similar between HUJI and CL cases, suggesting that both microphysics schemes agree on the amount of water that should condense for this injection rate. The differences in *T*, *RH*, and *LWC* are self-consistent, which is closely related to the cloud microphysical properties and droplet size distribution, as discussed next.

Figure 2 shows the time series of domain-averaged cloud microphysical properties, including droplet number concentration (N_d), mean droplet radius (r_d), effective radius (r_{eff}), and standard deviation of droplet size distribution (σ_r). It is interesting to see that droplet number concentration is sensitive to different advection schemes, and simulation with the advection scheme that suffers more from numerical diffusion tends to have a lower droplet number concentration. r_d, r_{eff}, and σ_r are not sensitive to the advection schemes. Results are consistent with the thermodynamics, because more cloud droplets of the same side (i.e., larger N_d and same r_d) suggests more condensed water (higher *LWC*), which can release more latent heat, and thus leads to a higher T and lower *RH* as shown in Figure 1. For cross comparison, r_d, r_{eff}, and σ_r in the CL-based cases are all smaller than those in the HUJI-based cases. This systematic difference in mean droplet size reflects differences in droplet size distributions

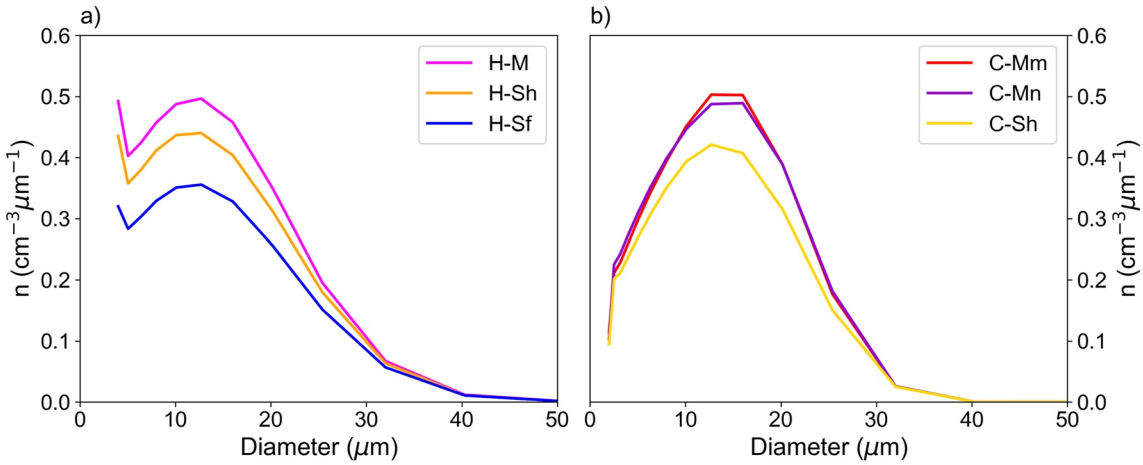

Figure 3. Spatially and temporally averaged droplet size distribution based on the (a) HUJI and (b) CL microphysics schemes with the different advection schemes indicated in the legend (see Table 1).

as shown in Figure 3: droplet size distributions in the CL-based cases are narrower due to the fact that the CL scheme is less computationally diffusive compared with the HUJI scheme. Note that distributions in Figure 3 are mean steady-state distributions, averaged spatially (over the whole domain) and temporally (between 0.5 and 1 hr every 5 min). It is also interesting to see that results from C-Mm, in which the total condensed water in the simulation domain is not conserved during advection, are statistically similar to those from C-Mn, in which the total mass is conserved, suggesting that the mass adjustment with MPDATA has negligible impacts on the simulation while maintaining conservation of mass.

3.2. Sensitivity to Aerosol Injection Rates

Three aerosol injection rates—0.25 cm^{-3} s^{-1} used above, 2.5 cm^{-3} s^{-1}, and 25 cm^{-3} s^{-1}, labeled as "clean", "normal", and "polluted"—are employed to explore the sensitivity to aerosol amount. For each case, variables (e.g., T) fluctuate in time and space while in steady state. We generate box and whisker plots of variables to show their statistical properties at steady state (between 0.5 and 1 hr) as shown in Figures 4 and 5. Each box covers data between 25% and 75% with the median value indicated by the white horizontal line at the center, and whiskers indicating data between the 5th and 95th percentiles. We first check the trend of each variable by changing the aerosol injection rate (e.g., H-M for the clean case vs. H-M for the normal case vs. H-M for the polluted case). Results show that T increases with increasing aerosol injection rate (Figures 4a and 4e) while Q_v is largely insensitive to aerosol injection rate (Figures 4b and 4f). A larger aerosol injection rate results in a higher *LWC* (Figures 4d and 4h), more cloud droplets (Figures 5a and 5e), smaller droplet sizes (Figures 5b, 5c, 5f, 5g), and a narrower size distribution (Figures 5d and 5h), which are all consistent with the chamber observations (Chandrakar et al., 2016). We then compare the differences that result from changing the advection schemes while using the same microphysics scheme and aerosol injection rates (e.g., H-M vs. H-Sh vs. H-Sf for the polluted case). Results show that the general trends are similar to those in Section 3.1: cases using advection schemes that have stronger numerical diffusion tend to predict lower T, higher *RH*, smaller *LWC*, and lower N_d. At the same time, r_d, r_{eff}, and σ_r are slightly larger when using advection schemes that have stronger numerical diffusion for the polluted condition case, while they are not sensitive to the advection scheme in the clean case as shown in Section 3.1. This phenomenon is due to the enhanced differences in N_d among cases for the polluted condition (Figures 5a and 5e). Note that N_d is plotted on a log scale and the absolute difference in N_d between cases (e.g., H-M vs. H-Sf) is much larger for the polluted case than in the clean case. Larger differences in N_d make the differences in r_d, r_{eff}, and σ_r distinguishable for the polluted case. In addition, we compare the sensitivity to changing the advection schemes and aerosol injection rate (e.g., simulations for the clean case vs. simulations for the normal case vs. simulations for the polluted case). Results show that all variables except *RH* become more sensitive to the changes in the advection scheme as the aerosol injection rate increases. *RH* is less sensitive in the polluted case because it is buffered to about 100% under polluted conditions. For cross comparison (e.g., the HUJI cases vs. the

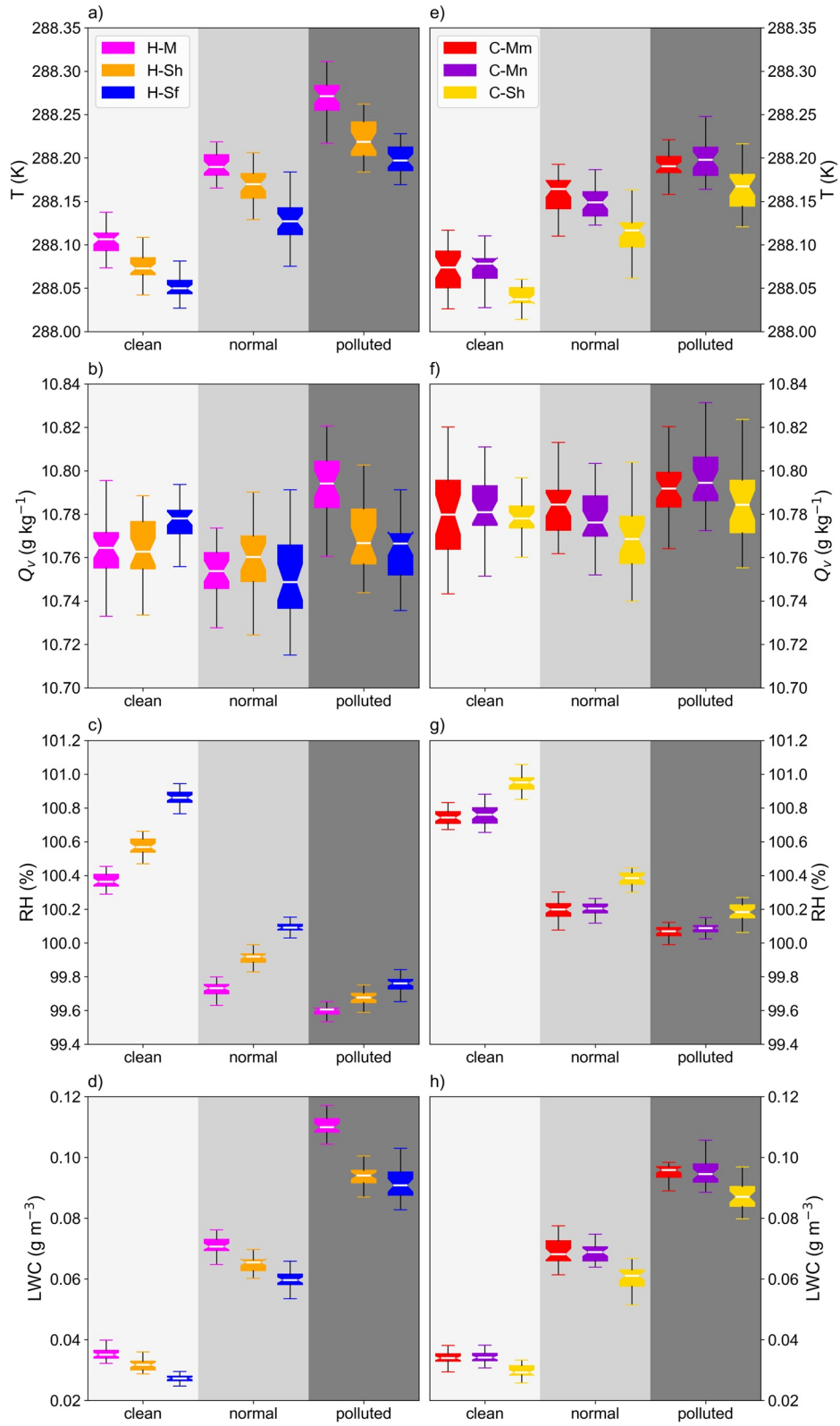

Figure 4. Box plots of domain-averaged T, Q_v, RH, and LWC between 0.5 and 1.0 hr for three different aerosol injection rates: 0.25 cm^{-3} s^{-1} (clean), 2.5 cm^{-3} s^{-1} (normal), and 25 cm^{-3} s^{-1} (polluted).

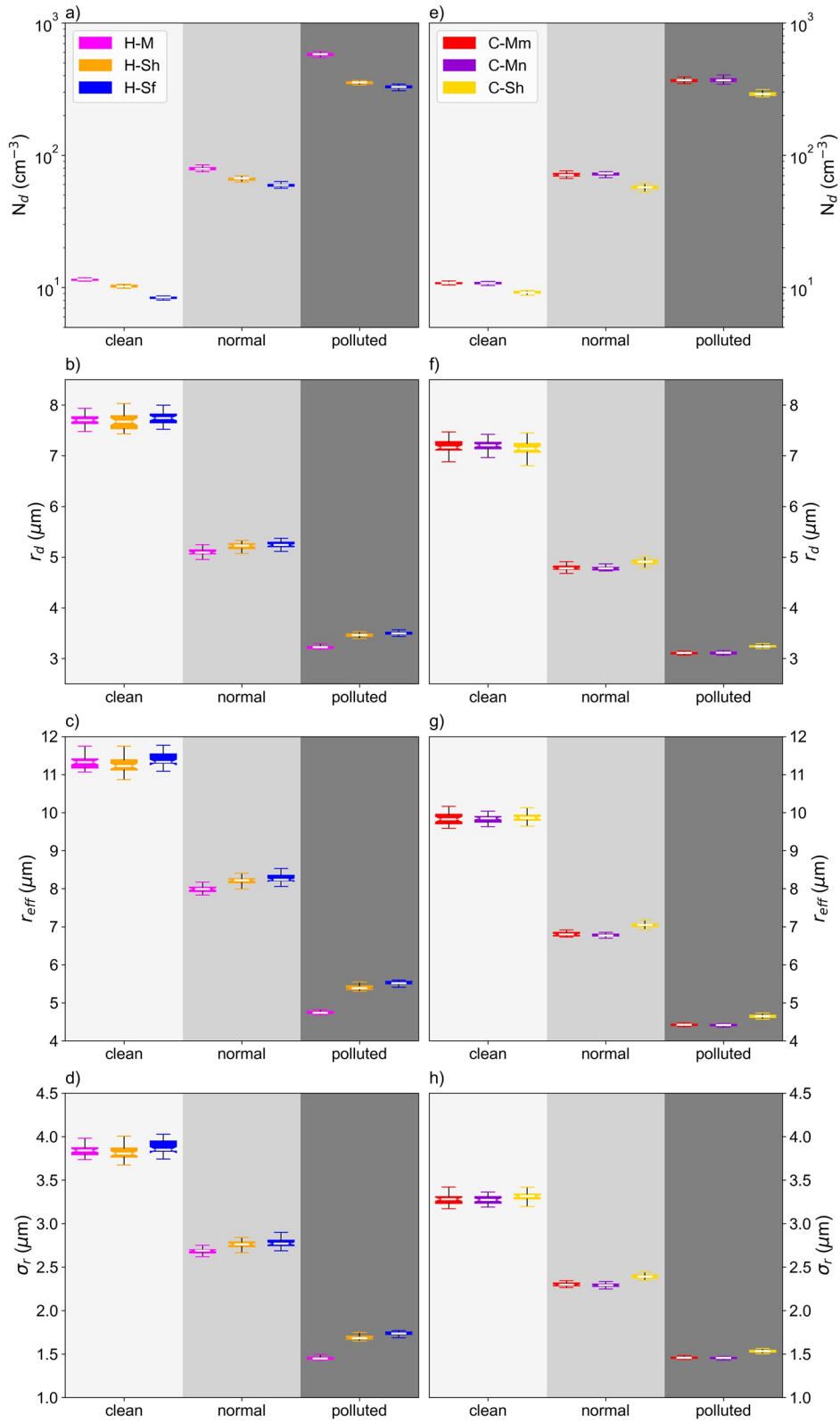

Figure 5. Box plots of domain-averaged N_d, r_d, r_{eff}, and σ_r between 0.5 and 1.0 hr for three different aerosol injection rates: 0.25 cm^{-3} s^{-1} (clean), 2.5 cm^{-3} s^{-1} (normal), and 25 cm^{-3} s^{-1} (polluted).

Table 2
Summary of Sensitivity Tests to Mass Adjustment, Minimal Droplet Size, and Bin Resolution

Case Name	Adjustment Factor	Minimal Droplet Radius (μm)	Bin Number
(legend in Figures 6–8)			(mass ratio)
C-Mm (control)	0.01	1	33 (2)
C-Mm-0.1a (0.1 adj)	0.1	1	33 (2)
C-Mm-2 μm (2 μm)	0.01	2	33 (2)
C-Mm-66b (66 bins)	0.01	1	66 ($2^{0.5}$)
C-Mm-132b (132 bins)	0.01	1	132 ($2^{0.25}$)

Note. Case setups are detailed in the main text.

CL cases), we note that the systematic differences between the HUJI-based cases and the CL-based cases hold for *RH*, *LWC*, and N_d in the polluted case, but diminish for r_d, r_{eff}, and σ_r.

Significant differences in N_d for different combinations of microphysics and advection schemes are noticeable in Figures 5a and 5e. For the smallest aerosol injection rate (0.25 cm^{-3} s^{-1}), N_d for the HUJI-based and CL-based cases can vary by a factor of over 1.5. Because all injected aerosols are activated as cloud droplets in clean conditions, the difference in N_d is due to the different microphysics and advection schemes; however, for the greatest aerosol injection rate (25 cm^{-3} s^{-1}), newly injected aerosol at low supersaturation might not activate into cloud droplets and thus accumulate in the chamber. Note that aerosols might not all activate into cloud droplets—even when turbulent fluctuations cause supersaturations greater than the aerosol's critical supersaturation—if there is insufficient extra water vapor available to activate all aerosols. Otherwise, high-frequency oscillations in cloud droplet number concentration could occur the following way: (a) a temporary high supersaturation activates all monodisperse aerosols into cloud droplets; (b) the large amount of newly formed cloud droplets lead to subsaturation in the next time step, which evaporates cloud droplets; (c) evaporation of cloud droplets releases water vapor causing a high supersaturation that can serve to try activating all aerosol particles again. Such oscillation is analogue to the oscillation found in aerosol nucleation and growth processes (McGraw & Saunders, 1984). Therefore, the different ways of handling activation in the HUJI-based cases and the CL-based cases can also lead to differences in N_d. In the HUJI-based cases, partial activation is not considered, meaning that all dry aerosols can be activated as cloud droplets based on the Köhler theory if the environmental supersaturation is larger than its critical supersaturation. In the CL-based cases, all dry aerosols can be activated as cloud droplets in relatively clean conditions. If the activation of all aerosols leads to a subsaturation, partial activation is on, meaning that only 20% of the dry aerosols can be activated as cloud droplets such that the supersaturation is still positive after activation. It can explain why the domain averaged RH is lower (Figure 4c) and N_d is larger (Figure 5a) under polluted conditions in the HUJI-based cases compared with the CL-based cases. Note that although the domain-averaged supersaturation in the polluted condition is smaller (even below 100% in the HUJI-based cases due to subsaturated side walls) than the critical supersaturation of monodisperse aerosol in polluted conditions, droplets can still be activated close to bottom or top surfaces where high supersaturation exists (Chandrakar et al., 2020), or through supersaturation fluctuations in a turbulent environment (Prabhakaran et al., 2020).

3.3. Sensitivity to Parameters in the Bin Microphysics Scheme

Chamber simulation results might depend on several parameters in the microphysics scheme. For example, for the mass adjustment method discussed in 2.2.1, the mass mixing ratio in a bin is adjusted if the mean droplet size is outside of the bin boundary, by setting the slope of the linear distribution such that the intersection is about 0.01 (defined as adjustment factor here) of the bin width. In addition, for all the CL-based schemes, the initial droplet radius is set to 1 μm, while the minimal droplet radius for the HUJI-based schemes is 2 μm as was also used in our previous study (Thomas et al., 2019). Lastly, mass-doubling bins (a total of 33 bins) are used in the above model intercomparisons. So, does the chamber simulation depend on the adjustment factor? Does the change of the minimal droplet radius affect the chamber simulation? Are results sensitive to the bin resolution? To address those questions, we choose C-Mm as the control case and employ several sensitivity tests. Specifically, we change the adjustment factor to 0.1 (C-Mm-0.1a), the minimal droplet radius to 2 μm (C-Mm-2 μm), the mass ratio to $2^{0.5}$ yielding 66 bins (C-Mm-66b) and to $2^{0.25}$ yielding 132 bins (C-Mm-132b). Table 2 summarizes the case names and key parameters. Results show that volume-average thermodynamic variables, that is, T and Q_v, as well as *RH* and *LWC*, are insensitive to those changes as shown in Figure 6. In contrast, volume-average microphysical properties show larger case-by-case variations, as shown in Figure 7. For example, N_d becomes smaller when we increase the minimal droplet radius from 1 μm to 2 μm.

It is interesting to note that droplet sizes and spectral widths increase with the increase in bin resolution (Figure 7). Spatially and temporally averaged droplet size distribution also confirm that the distribution becomes broader with the increase in bin resolution as shown in Figure 8. This observation contradicts our initial expectation that

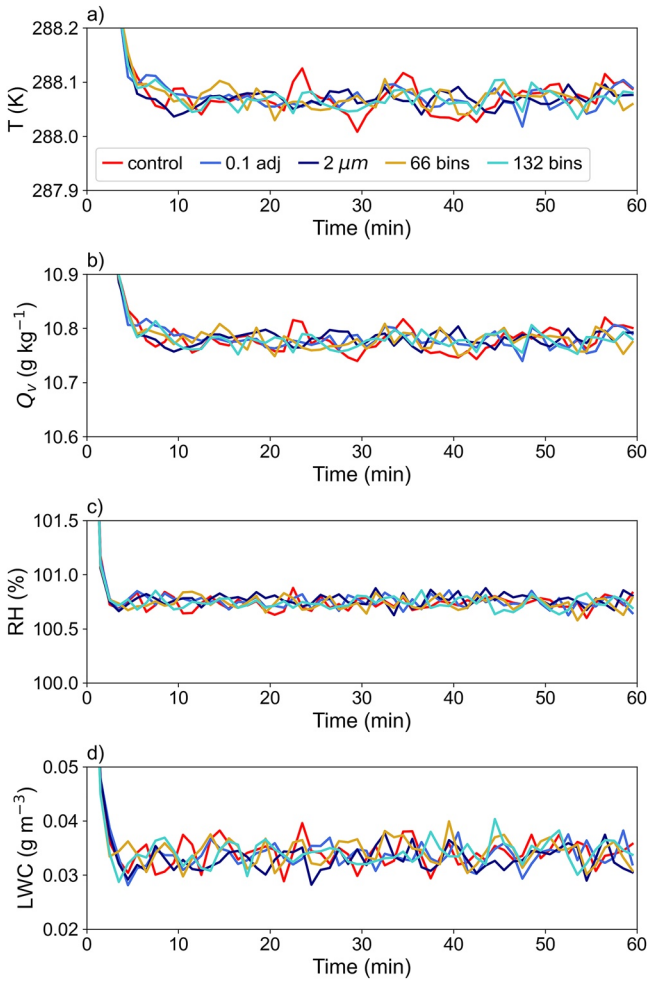

Figure 6. Time series of domain-averaged (a) temperature, (b) water vapor mixing ratio, (c) relative humidity, and (d) liquid water content in a simulated convection cloud chamber. Results from the control case are the same as C-Mm in Figure 1. The other cases are sensitivity tests for the adjustment factor, minimal droplet radius, and bin resolution. Case setups are detailed in the main text and Table 2.

droplet size distribution should become narrower with increasing bin resolution, due to less numerical diffusion in the droplet radius space. To explore this counterintuitive result, we conduct three sets of simulations using the CL scheme with three different resolutions as before (33 bins, 66 bins, and 132 bins). We will show below that the broadening of the droplet size distribution when refining microphysical bins is due to advection of hydrometeors.

First, we perform an idealized simulation for which all droplets grow by condensation in a still environment without advection and sedimentation. The environmental temperature and water vapor mixing ratio are set as constants with values of $T = 293\ K$ and $q_v = 0.18\ \mathrm{g\,kg^{-1}}$, corresponding to a supersaturation of 22.3%. Droplet number concentration is 100 cm^{-3} and all droplets are initially located in the smallest bin. Note that aerosols are only added at the beginning of the simulation in this case, so there is no continuous injection of aerosols. This is a way to check whether our algorithm for calculating droplet condensational growth is correct because the analytical solution for the droplet growth is known for a constant supersaturation environment. The total simulation time is 20 s with a time step of 0.02 s. Figure S1 in Supporting Information S1 shows that the droplet size distribution is indeed narrower for a higher bin resolution, consistent with our initial expectation, and the time evolution of the mode of the distribution agrees well with the analytical value.

We then conduct a box model simulation for which the liquid water static energy and total water mixing ratio are 293.4 K and 17 g kg^{-1}, both held constant, resulting an initial supersaturation of 12.7%. Monodisperse aerosols with a dry radius of 62.5 nm are injected into the box at a constant rate of 0.25 cm^{-3}s^{-1}. Dry aerosols are activated into cloud droplets and experience condensational growth under supersaturated conditions. Droplets are removed in a simple way based on their terminal velocity

$$N_d = N_d \left(1 - \frac{dt}{\tau}\right) \tag{4}$$

where N_d is the droplet number concentration in one bin, dt is the time step, and τ is the characteristic time for droplet sedimentation $\tau = H/v_t$. H can be considered to be the chamber height (1 m here) and v_t is the terminal velocity of droplets in that bin. Basically, this is a simple zero-dimensional model to mimic the steady state in the convection cloud chamber. The droplet size distribution reaches steady state after a few minutes when the injection rate equals to the removal rate due to sedimentation. Figure S2 in Supporting Information S1 shows that the droplet size distributions are similar with different bin resolutions, and refining the bins does not lead to a broader distribution.

Finally, we conduct chamber simulations as before (i.e., Figure 8) except that we change the subsaturated wall condition to an adiabatic wall condition. We create an adiabatic wall condition by turning off the scalar fluxes (e.g., temperature and water vapor mixing ratio) at the side walls. Because both bottom and top surfaces are saturated with respect to water at two different temperatures, through turbulent mixing, the whole chamber is supersaturated with a domain-averaged saturation ratio that is much higher than that for the subsaturated wall condition. For comparison, when side walls are subsaturated, air close to the side wall is likely to be subsaturated due to the sink of water vapor near the wall and the domain-averaged supersaturation is much lower. Note that subsaturated wall condition is chosen for all other simulations in this study so the domain-averaged supersaturation without cloud droplets is close to the in situ measurements in Pi chamber (Chandrakar et al., 2016). Changing to an adiabatic wall condition forces the whole chamber to be supersaturated, and thus evaporation of droplets is negligible. Figure S3 in Supporting Information S1 shows that all three resolutions agree for smaller droplets much better than in Figure 8 but still differ for larger droplets, with a broader distribution for higher resolutions,

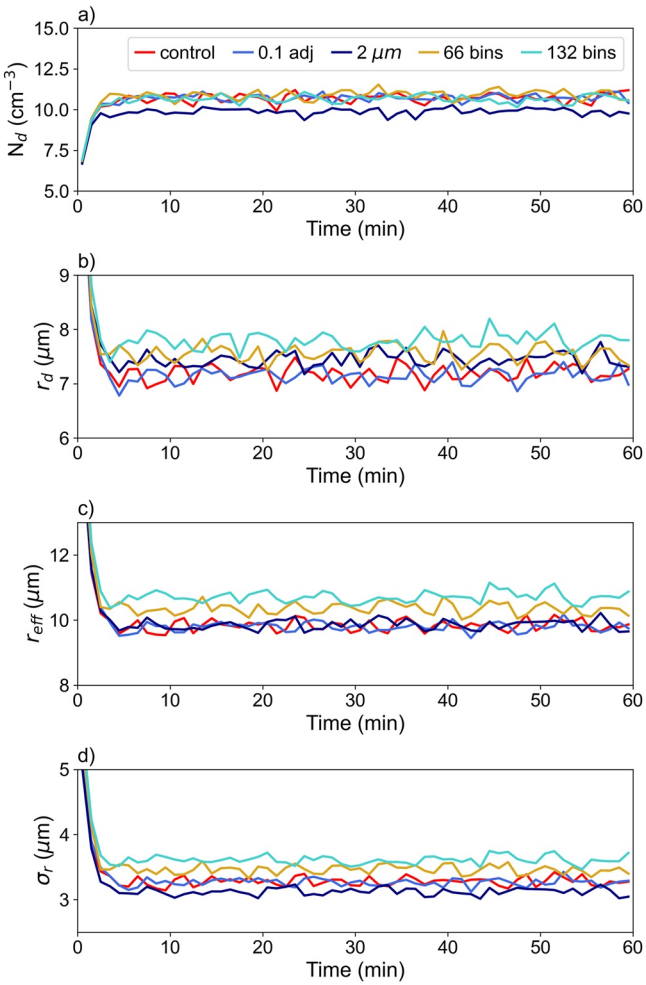

Figure 7. Time series of domain-averaged (a) droplet number concentration, (b) mean droplet radius, (c) effective radius, and (d) standard deviation of droplet size distribution in a simulated convection cloud chamber. Results from the control case are the same as C-Mm in Figure 2. Other cases are sensitivity tests for the adjustment factor, minimal droplet radius, and bin resolution. Case setups are detailed in the main text and Table 2.

suggesting that the spectra broadening is not due to evaporation or side-wall effects.

In short, we only see the broadening of the distribution when refining bin widths for the 3D chamber simulations, suggesting that the broadening with bin refinement is due to the transport of the hydrometeors. Transport of hydrometeors in the simulation can be affected by advection, diffusion, and sedimentation. Superficially, the broadening found in this study is similar to the broadening found in Morrison et al. (2018). More research is needed to explore the broadening at a fundamental level; however, this series of tests clearly points to transport as being the cause.

3.4. Sensitivity to Spatial and Temporal Resolutions

All above simulations, as well as simulations in Thomas et al. (2019), use a spatial resolution of $dx = dy = dz = 3.125\ cm$ and a time step of 0.02 s. We test the sensitivity of Pi chamber simulations to different spatial and temporal resolutions, which has not been done before. Two cases (H-M and C-Mm) are chosen to simulate the Pi chamber at three other spatial resolutions (6.25 cm, 12.5 cm, and 25 cm) and two temporal resolutions (0.01 and 0.04 s) with the same initial and boundary conditions. Note that spatial resolutions are changed in all three directions. Results are shown in Figures S4 (H-M) and S5 (C-Mm) in Supporting Information S1. The behaviors of H-M and C-Mm are similar at different resolutions. Specifically, results are not sensitive to temporal resolution but refining the grid spacing up to 3.125 cm has a considerable impact on dynamical, thermodynamical, and microphysical properties. The increase of the turbulence strength (energy dissipation rate and turbulent kinetic energy) is mainly due to the increase in surface fluxes. The change in surface heat fluxes with the change in grid spacing is because of the simplified parameterization of surface fluxes in large-eddy simulations based on Monin-Obukhov similarity theory. A smaller grid spacing leads to a larger gradient in temperature and water vapor mixing ratio between surface and the adjacent air, leading to larger calculated sensible and latent heat fluxes. Direct numerical simulations are needed to fully resolve the surface layer and test the convergence with respect to spatial grid spacing in future studies.

The decrease in temperature, water vapor mixing ratio, droplet number concentration, and mean droplet size with increased spatial resolution are not mainly due to the change of the turbulence strength but, instead, arise from having subsaturated side walls. To show the impact, we conduct simulations with adiabatic side walls at different spatial resolutions and the results are shown in Figures S6 (H-M) and S7 (C-Mm in Supporting Information S1). It can be seen that changes in energy dissipation rate and turbulent kinetic energy with spatial resolution are similar to those with subsaturated walls (Figures S4 and S5 in Supporting Information S1), but the thermodynamic and microphysical properties are not sensitive to spatial resolution. Our results suggest that, at least when using our current model setup to simulate the Pi chamber, a courser resolution (up to about 10 cm) is sufficient to obtain convergence for thermodynamic and microphysical properties under adiabatic wall conditions. It should be mentioned that sensitivities found in this section do not change our conclusion in previous sections, in which we used the same initial and boundary conditions as well as temporal and spatial resolutions.

4. Conclusions and Implications

An atmospheric large-eddy simulation model with the HUJI scheme has been modified to simulate a convection cloud chamber (Thomas et al., 2019). In this study, we presented results from intercomparison studies of large-eddy simulations of steady-state clouds in the Pi chamber using two microphysics schemes and different

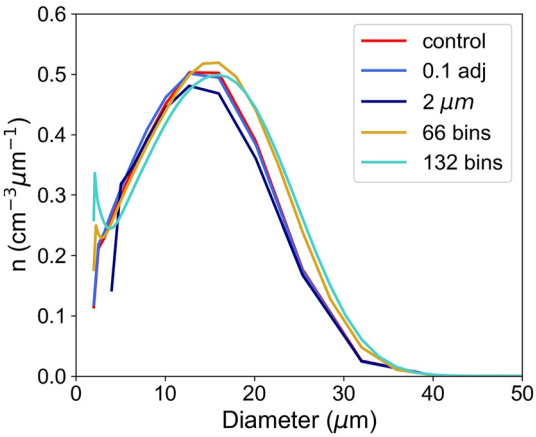

Figure 8. Spatially and temporally averaged droplet size distribution. The distribution from the control case is the same as C-Mm in Figure 3. The other cases are sensitivity tests for the adjustment factor, minimal droplet radius, and bin resolution. Case setups are detailed in the main text and Table 2.

advection methods. Pi chamber simulation with the setup of observationally guided initial and boundary conditions provides a unique framework to test the sensitivity of simulations to the different schemes at the laboratory scale. Specifically, the CL scheme, based on the method of moments, has also been implemented for chamber simulations. However, it is not straightforward to implement the CL scheme in a 3-D model because the MPDATA advection scheme currently used in the model does not preserve the interrelationship of the two prognostic variables (number and mass mixing ratio) after advection. To properly transport hydrometeors in the CL scheme, several advection methods were tested, including the MPDATA scheme with mass and number adjustments, and the Lagrangian advection scheme with a hybrid option. For comparison, we applied the same advection methods to the HUJI scheme, and also included the Lagrangian advection scheme with first-order linear advection. Note that all simulations were done using the same dynamic model with identical initial and boundary conditions. In this way, our simulations can help to diagnose the roles of the microphysics and advection schemes by ruling out other factors, such as subgrid and surface flux parameterizations.

Results show that spectral bin microphysics schemes and the treatment of advection can alter the statistical properties of simulated clouds. By sorting the cases by the estimated degree of numerical diffusion, we find that, when using the same microphysics scheme, simulation with the advection scheme that suffers more from numerical diffusion along the size coordinate tends to have a lower temperature, higher relative humidity, smaller liquid water content, and more droplet number concentration. Results are self-consistent, because more cloud droplets in the convection chamber are related to more condensed water, which releases more latent heat, and thus leads to a higher temperature and lower relative humidity. In addition, simulation with the microphysics scheme that suffers more from numerical diffusion tends to have a broader distribution and thus larger mean droplet sizes. We also find that refining microphysical bin widths leads to a broader droplet size distribution. The broadening effect arises from hydrometeor transport, which shows some similarity to the broadening effect reported in Morrison et al. (2018) for atmospheric cloud simulations. For a constant aerosol injection rate of 0.25 $cm^{-3}\ s^{-1}$, N_d can differ by about a factor of 1.5 between the largest and smallest values when using different advection schemes. Simulated clouds can have similar N_d by choosing different combinations of microphysics and advection schemes. A larger aerosol injection rate leads to a higher T due to latent heat release from more condensed water (LWC), more cloud droplets (N_d), smaller droplet sizes (r_d), and narrower size distributions (σ_r). Results show that all variables expect one (RH) are more sensitive to the changes of the advection scheme as the increase of aerosol injection rate. RH is less sensitive in the polluted condition because it is buffered to about 100% under polluted conditions. Aerosols are monodisperse in our simulation (all dry aerosols in one bin), and the simple Boolean treatment of activation based on the Köhler theory (i.e., all dry aerosols in that bin are activated or not contingent on the environmental supersaturation) would lead to unrealistic oscillations in simulated clouds under polluted conditions. Such oscillation can be avoided by considering partial activation, in which only a fraction of the dry aerosol can be activated as cloud droplets. The way to handle partial activation in the model can also affect the simulated cloud properties, especially for N_d.

Our conclusion that changes in advection schemes can produce similar variability in simulated cloud properties as changes in microphysics schemes for chamber simulations contradicts to some recent studies (Gavze et al., 2020; Lynn et al., 2021). For example, Lynn et al. (2021) compared simulations of a supercell storm using several microphysics and advection schemes at different scales, and they found that results agree well when using the same spectral bin microphysics schemes and different advection schemes, but huge differences are found when using the same advection scheme and different bulk microphysics schemes. Their results show that cloud and precipitation show much higher sensitivity to microphysical schemes than to advection schemes. Several reasons might contribute to this inconsistency. First, two bin microphysics schemes are used in this study, while one bin microphysics scheme and several bulk microphysics schemes are used in Lynn et al. (2021). It is expected that the two bin microphysics schemes are more similar when compared with bulk microphysics schemes. Second, hydrometeors and microphysical processes occurring in a cloud convection chamber are much simpler compared with those in a supercell storm. For example, drizzle, rain, ice crystals, hail, and snow do not exist in the chamber

and those hydrometeors and associated processes are treated quite differently in different microphysics schemes. Lastly, spatial and temporal resolutions for chamber simulations are much finer compared with simulations in the atmosphere, and therefore, the comparative effect of advection on microphysical variables may be larger. In short, we consider this study as complementary to, rather than contradictory to other model intercomparison studies; aside from the fact that all those studies talk about different microphysics and advection schemes, there is not much else in common among them in terms of model setups and simulated conditions. Results from this study can help us better understand the variations in chamber simulations when using different schemes, which is of interest to the cloud physics community in general, as well as to facilitate the design of future large-scale cloud chambers (Shaw et al., 2020). One should be cautious, however, when extending the conclusions of this study to simulations of natural cloud systems due to the additional complexities involved there.

Domain-averaged RH and N_d in the steady state show an anticorrelation using various advection methods with the same microphysics scheme (Figures 1c and 1g and Figures 2a and 2e). Chandrakar et al. (2018) derived an analytical expression of mean supersaturation in a convection cloud chamber at the steady state: $\overline{s} = s_0\tau_s/\tau_t$ (Equation 12 in that paper). Here, s_0 is the supersaturation without cloud droplets, and τ_s is the global system time scale $\tau_s = \tau_c\tau_t/(\tau_c + \tau_t)$. τ_t is the turbulent mixing time scale, which can be considered as a constant for Rayleigh-Bénard convection (e.g., same temperature difference between top and bottom surfaces). τ_c is the phase relaxation time, which is inversely proportional to the first moment of droplet size distribution, $\tau_c \propto \left(\overline{r}N_d\right)^{-1}$. Because $\overline{r_d}$ shows much less variation for different advection schemes, a larger N_d leads to a smaller τ_c, resulting in a smaller τ_s, and thus a smaller $\overline{s}$ (note that $\overline{RH} = \overline{s} + 1$).

Do we know which combination of microphysics and advection scheme is the best for cloud chamber simulation? Unfortunately, we cannot answer this question at this moment because of a lack of observational data for comparison. Although our model setup is based on the chamber setup and observations in Chandrakar et al. (2016), some assumptions and simplifications are made for our simulations. For example,: (a) aerosols are injected in all grid boxes in the model, but they are injected at one point in the real chamber; (b) assumptions are made for the surface and wall conditions to calculate heat and water vapor fluxes, but there is no direct measurement to evaluate those fluxes; and (c) droplets are removed from the simulated domain if they totally evaporate or sediment out but, in the real chamber, droplets may also be lost at the wall surface and, when droplets totally evaporate, they deactivate as haze particles and can be reactivated again if the environmental supersaturation is larger than its critical supersaturation. Even so, the model intercomparisons in this study provide some new aspects to design future experiments to constrain the modeling results in the future. For example, for the low aerosol injection rate, only N_d shows considerable case-by-case variation, suggesting that rigorous experiments and precise observations are needed for model evaluation for relatively clean conditions. For the high aerosol injection rate, LWC also differs considerably, which might be a good variable for model evaluation.

Our next step is to evaluate model simulations with improved in situ measurements. A convection cloud chamber provides an ideal environment for model intercomparisons and evaluation because it has well-characterized boundary conditions, it creates statistically steady-state conditions, and the flow does not respond significantly to changes in the microphysics. We also look forward to seeing more Pi Chamber simulations, in which more numerical and theoretical models are applied to simulate the convection cloud chamber with the same initial and boundary conditions. Comparisons of simulations with various microphysics and advection schemes can help us better understand uncertainties in simulations of clouds in the chamber and the real atmosphere.

Data Availability Statement

The SAM model is available from Dr. Marat Khairoutdinov of Stony Brook University (http://rossby.msrc.sunysb.edu/marat/SAM.html). The model setup, input files, and outputs are available upon request to the first author.

Acknowledgments
This work was supported primarily by the U.S. Department of Energy's Atmospheric System Research, an Office of Science Biological and Environmental Research program. Brookhaven National Laboratory is operated by the DOE by Brookhaven Science Associates under contract DE-SC0012704. Pacific Northwest National Laboratory is operated by Battelle for the U.S. Department of Energy under Contract DE-AC05-76RL01830. The MTU authors acknowledge support from National Science Foundation Grant AGS-1754244. We thank Dr. Ehud Gavze (Hebrew University of Jerusalem) for providing the semi-Lagrangian advection code and Dr. Kobby Shpund (Pacific Northwest National Laboratory) for valuable discussions. The authors also appreciate discussions with Graham Feingold, Hugh Morrison, and Mikael Witte.

References

Beard, K. V. (1976). Terminal velocity and shape of cloud and precipitation drops aloft. *Journal of the Atmospheric Sciences*, *33*(5), 851–864. https://doi.org/10.1175/1520-0469(1976)033<0851:TVASOC>2.0.CO;2

Chandrakar, K. K., Cantrell, W., Chang, K., Ciochetto, D., Niedermeier, D., Ovchinnikov, M., et al. (2016). Aerosol indirect effect from turbulence-induced broadening of cloud-droplet size distributions. *Proceedings of the National Academy of Sciences*, *113*(50), 14243–14248. https://doi.org/10.1073/pnas.1612686113

Chandrakar, K. K., Cantrell, W., Krueger, S., Shaw, R. A., & Wunsch, S. (2020). Supersaturation fluctuations in moist turbulent Rayleigh–Bénard convection: A two-scalar transport problem. *Journal of Fluid Mechanics*, *884*, A19. https://doi.org/10.1017/jfm.2019.895

Chandrakar, K. K., Cantrell, W., & Shaw, R. A. (2018). Influence of turbulent fluctuations on cloud droplet size dispersion and aerosol indirect effects. *Journal of the Atmospheric Sciences*, *75*(9), 3191–3209. https://doi.org/10.1175/JAS-D-18-0006.1

Chang, K., Bench, J., Brege, M., Cantrell, W., Chandrakar, K., Ciochetto, D., et al. (2016). A laboratory facility to study gas–aerosol–cloud interactions in a turbulent environment: The Π chamber. *Bulletin of the American Meteorological Society*, *97*(12), 2343–2358. https://doi.org/10.1175/BAMS-D-15-00203.1

Chen, J.-P., & Lamb, D. (1994). Simulation of cloud microphysical and chemical processes using a multicomponent framework. Part I: Description of the microphysical model. *Journal of the Atmospheric Sciences*, *51*(18), 2613–2630. https://doi.org/10.1175/1520-0469(1994)051<2613:SOCMAC>2.0.CO;2

Fan, J., Ovchinnikov, M., Comstock, J. M., McFarlane, S. A., & Khain, A. (2009). Ice formation in Arctic mixed-phase clouds: Insights from a 3-D cloud-resolving model with size-resolved aerosol and cloud microphysics. *Journal of Geophysical Research*, *114*(D4), D04205. https://doi.org/10.1029/2008JD010782

Gavze, E., Ilotoviz, E., & Khain, A. (2020). A computationally efficient linear semi-Lagrangian scheme for the advection of microphysical variables in cloud-resolving models. *Monthly Weather Review*, *148*(8), 3427–3452. https://doi.org/10.1175/MWR-D-19-0080.1

Grabowski, W. W. (2019). Separating physical impacts from natural variability using piggybacking (master-slave) technique. *Advances in Geosciences*, *49*, 105–111. https://doi.org/10.5194/adgeo-49-105-2019

Grabowski, W. W. (2020). Comparison of Eulerian bin and Lagrangian particle-based schemes in simulations of Π chamber dynamics and microphysics. *Journal of the Atmospheric Sciences*, *77*(3), 1151–1165. https://doi.org/10.1175/JAS-D-19-0216.1

Grabowski, W. W., Morrison, H., Shima, S.-I., Abade, G. C., Dziekan, P., & Pawlowska, H. (2019). Modeling of cloud microphysics: Can we do better? *Bulletin of the American Meteorological Society*, *100*(4), 655–672. https://doi.org/10.1175/BAMS-D-18-0005.1

Hill, A., Shipway, B., & Boutle, I. (2015). How sensitive are aerosol-precipitation interactions to the warm rain representation? *Journal of Advances in Modeling Earth Systems*, *7*(3), 987–1004. https://doi.org/10.1002/2014MS000422

Hoffmann, F., Raasch, S., & Noh, Y. (2015). Entrainment of aerosols and their activation in a shallow cumulus cloud studied with a coupled LCM–LES approach. *Atmospheric Research*, *156*, 43–57. https://doi.org/10.1016/j.atmosres.2014.12.008

Khain, A., Beheng, K., Heymsfield, A., Korolev, A., Krichak, S., Levin, Z., et al. (2015). Representation of microphysical processes in cloud-resolving models: Spectral (bin) microphysics versus bulk parameterization. *Reviews of Geophysics*, *53*(2), 247–322. https://doi.org/10.1002/2014RG000468

Khain, A., Lynn, B., & Dudhia, J. (2010). Aerosol effects on intensity of landfalling hurricanes as seen from simulations with the WRF model with spectral bin microphysics. *Journal of the Atmospheric Sciences*, *67*(2), 365–384. https://doi.org/10.1175/2009JAS3210.1

Khain, A., Pokrovsky, A., Pinsky, M., Seifert, A., & Phillips, V. (2004). Simulation of effects of atmospheric aerosols on deep turbulent convective clouds using a spectral microphysics mixed-phase cumulus cloud model. Part I: Model description and possible applications. *Journal of the Atmospheric Sciences*, *61*(24), 2963–2982. https://doi.org/10.1175/JAS-3350.1

Khain, A., & Sednev, I. (1996). Simulation of precipitation formation in the Eastern Mediterranean coastal zone using a spectral microphysics cloud ensemble model. *Atmospheric Research*, *43*(1), 77–110. https://doi.org/10.1016/S0169-8095(96)00005-1

Khairoutdinov, M. F., & Randall, D. A. (2003). Cloud resolving modeling of the ARM summer 1997 IOP: Model formulation, results, uncertainties, and sensitivities. *Journal of the Atmospheric Sciences*, *60*(4), 607–625. https://doi.org/10.1175/1520-0469(2003)060<0607:CRMOTA>2.0.CO;2

Kuan-Ting, O., Wood, R., & Bretherton, C. S. (2018). Ultraclean layers and optically thin clouds in the stratocumulus-to-cumulus transition. Part II: Depletion of cloud droplets and cloud condensation nuclei through collision–coalescence. *Journal of the Atmospheric Sciences*, *75*(5), 1653–1673. https://doi.org/10.1175/JAS-D-17-0218.1

Lynn, B., Gavze, E., Dudhia, J., Gill, D., & Khain, A. (2021). A fast linear semi-Lagrangian advection scheme coupled with spectral (bin) microphysics to simulate an idealized super cell storm in WRF. *Monthly Weather Review*. https://doi.org/10.1175/MWR-D-20-0244.1

Lynn, B., Khain, A. P., Dudhia, J., Rosenfeld, D., Pokrovsky, A., & Seifert, A. (2005). Spectral (bin) microphysics coupled with a mesoscale model (MM5). Part II: Simulation of a CaPE rain event with a squall line. *Monthly Weather Review*, *133*(1), 59–71. https://doi.org/10.1175/MWR-2841.1

McGraw, R. (2007). Numerical advection of correlated tracers: Preserving particle size/composition moment sequences during transport of aerosol mixtures. *Journal of Physics: Conference Series*, *78*(1), 012045. https://doi.org/10.1088/1742-6596/78/1/012045

McGraw, R., & Saunders, J. H. (1984). A condensation feedback mechanism for oscillatory nucleation and growth. *Aerosol Science and Technology*, *3*(4), 367–380. https://doi.org/10.1080/02786828408959025

Morrison, H., van Lier-Walqui, M., Fridlind, A. M., Grabowski, W. W., Harrington, J. Y., Hoose, C., et al. (2020). Confronting the challenge of modeling cloud and precipitation microphysics. *Journal of Advances in Modeling Earth Systems*, *12*(8), e2019MS001689. https://doi.org/10.1029/2019MS001689

Morrison, H., Witte, M., Bryan, G. H., Harrington, J. Y., & Lebo, Z. J. (2018). Broadening of modeled cloud droplet spectra using bin microphysics in an Eulerian spatial domain. *Journal of the Atmospheric Sciences*, *75*(11), 4005–4030. https://doi.org/10.1175/JAS-D-18-0055.1

Niedermeier, D., Voigtländer, J., Schmalfuß, S., Busch, D., Schumacher, J., Shaw, R. A., & Stratmann, F. (2020). Characterization and first results from LACIS-T: A moist-air wind tunnel to study aerosol–cloud–turbulence interactions. *Atmospheric Measurement Techniques*, *13*(4), 2015–2033. https://doi.org/10.5194/amt-13-2015-2020

Olesik, M., Arabas, S., Banaśkiewicz, J., Bartman, P., Baumgartner, M., & Unterstrasser, S. (2021). On numerical broadening of particle size spectra: A condensational growth study using PyMPDATA 1.0. *Geoscientific Model Development*, *15*, 3879–3899. https://doi.org/10.5194/gmd-15-3879-2022

Ovchinnikov, M., Ackerman, A. S., Avramov, A., Cheng, A., Fan, J., Fridlind, A. M., et al. (2014). Intercomparison of large-eddy simulations of Arctic mixed-phase clouds: Importance of ice size distribution assumptions. *Journal of Advances in Modeling Earth Systems*, *6*(1), 223–248. https://doi.org/10.1002/2013MS000282

Ovchinnikov, M., & Easter, R. C. (2009). Nonlinear advection algorithms applied to interrelated tracers: Errors and implications for modeling aerosol–cloud interactions. *Monthly Weather Review*, *137*(2), 632–644. https://doi.org/10.1175/2008MWR2626.1

Ovchinnikov, M., & Ghan, S. J. (2005). Parallel simulations of aerosol influence on clouds using cloud-resolving and single-column models. *Journal of Geophysical Research*, *110*(D15), D15S10. https://doi.org/10.1029/2004JD005088

Pardo, L. H., Morrison, H., Machado, L. A., Harrington, J. Y., & Lebo, Z. J. (2020). Drop size distribution broadening mechanisms in a bin microphysics Eulerian model. *Journal of the Atmospheric Sciences*, *77*(9), 3249–3273. https://doi.org/10.1175/JAS-D-20-0099.1

Prabhakaran, P., Shawon, A. S. M., Kinney, G., Thomas, S., Cantrell, W., & Shaw, R. A. (2020). The role of turbulent fluctuations in aerosol activation and cloud formation. *Proceedings of the National Academy of Sciences*, *117*(29), 16831–16838. https://doi.org/10.1073/pnas.2006426117

Rood, R. B. (1987). Numerical advection algorithms and their role in atmospheric transport and chemistry models. *Reviews of Geophysics*, *25*(1), 71–100. https://doi.org/10.1029/RG025i001p00071

Shaw, R. A., Cantrell, W., Chen, S., Chuang, P., Donahue, N., Feingold, G., et al. (2020). Cloud–aerosol–turbulence interactions: Science priorities and concepts for a large-scale laboratory facility. *Bulletin of the American Meteorological Society*, *101*(7), E1026–E1035. https://doi.org/10.1175/BAMS-D-20-0009.1

Shima, S.-I., Kusano, K., Kawano, A., Sugiyama, T., & Kawahara, S. (2009). The super-droplet method for the numerical simulation of clouds and precipitation: A particle-based and probabilistic microphysics model coupled with a non-hydrostatic model. *Quarterly Journal of the Royal Meteorological Society*, *135*(642), 1307–1320. https://doi.org/10.1002/qj.441

Shipway, B., & Hill, A. (2012). Diagnosis of systematic differences between multiple parametrizations of warm rain microphysics using a kinematic framework. *Quarterly Journal of the Royal Meteorological Society*, *138*(669), 2196–2211. https://doi.org/10.1002/qj.1913

Smolarkiewicz, P. K., & Grabowski, W. W. (1990). The multidimensional positive definite advection transport algorithm: Nonoscillatory option. *Journal of Computational Physics*, *86*(2), 355–375. https://doi.org/10.1016/0021-9991(90)90105-A

Stevens, B., Moeng, C.-H., Ackerman, A. S., Bretherton, C. S., Chlond, A., de Roode, S., et al. (2005). Evaluation of large-eddy simulations via observations of nocturnal marine stratocumulus. *Monthly Weather Review*, *133*(6), 1443–1462. https://doi.org/10.1175/MWR2930.1

Thomas, S., Ovchinnikov, M., Yang, F., van der Voort, D., Cantrell, W., Krueger, S. K., & Shaw, R. A. (2019). Scaling of an atmospheric model to simulate turbulence and cloud microphysics in the Π chamber. *Journal of Advances in Modeling Earth Systems*, *11*(7), 1981–1994. https://doi.org/10.1029/2019MS001670

Tzivion, S., Feingold, G., & Levin, Z. (1987). An efficient numerical solution to the stochastic collection equation. *Journal of the Atmospheric Sciences*, *44*(21), 3139–3149. https://doi.org/10.1175/1520-0469(1987)044<3139:AENSTT>2.0.CO;2

VanZanten, M. C., Stevens, B., Nuijens, L., Siebesma, A. P., Ackerman, A., Burnet, F., et al. (2011). Controls on precipitation and cloudiness in simulations of trade-wind cumulus as observed during RICO. *Journal of Advances in Modeling Earth Systems*, *3*(2). https://doi.org/10.1029/2011MS000056

Xue, L., Bera, S., Chen, S., Choudhary, H., Dixit, S., Grabowski, W. W., et al. (2022). Progress and challenges in modeling dynamics-microphysics interactions: From the Pi chamber to monsoon convection. *Bulletin of the American Meteorological Society*. https://doi.org/10.1175/BAMS-D-22-0018.1

Xue, L., Fan, J., Lebo, Z. J., Wu, W., Morrison, H., Grabowski, W. W., et al. (2017). Idealized simulations of a squall line from the MC3E field campaign applying three bin microphysics schemes: Dynamic and thermodynamic structure. *Monthly Weather Review*, *145*(12), 4789–4812. https://doi.org/10.1175/MWR-D-16-0385.1

Yamaguchi, T., Feingold, G., & Kazil, J. (2019). Aerosol-cloud interactions in trade wind cumulus clouds and the role of vertical wind shear. *Journal of Geophysical Research: Atmospheres*, *124*(22), 12244–12261. https://doi.org/10.1029/2019JD031073

Yamaguchi, T., Randall, D. A., & Khairoutdinov, M. F. (2011). Cloud modeling tests of the ULTIMATE–MACHO scalar advection scheme. *Monthly Weather Review*, *139*(10), 3248–3264. https://doi.org/10.1175/MWR-D-10-05044.1